ISSN 1995-0780, Nanotechnologies in Russia, 2017, Vol. 12, Nos. 3–4, pp. 174–184. © Pleiades Publishing, Ltd., 2017.
Original Russian Text © T.F. Sheshko, Yu.M. Serov, T.A. Kryuchkova, I.A. Khayrullina, I.V. Chislova, L.V. Yafarova, I.A. Zvereva, 2017, published in Rossiiskie Nanotekhnologii, 2017, Vol. 12, Nos. 3–4.

Study of Effect of Preparation Method and Composition on the Catalytic Properties of Complex Oxides $(Gd,Sr)_{n+1}Fe_nO_{3n+1}$ for Dry Reforming of Methane

T. F. Sheshko[a]*, Yu. M. Serov[a], T. A. Kryuchkova[a], I. A. Khayrullina[a], I. V. Chislova[b], L. V. Yafarova[b], and I. A. Zvereva[b]

[a] *RUDN University, Moscow, 117198 Russia*
[b] *St. Petersburg State University, St. Petersburg, 199034 Russia*
**e-mail: sheshko_tf@rudn.university*

Received March 26, 2016; in final form, December 13, 2016

Abstract—The catalytic activity of nanostructured perovskite-type ferrites of gadolinium and strontium, has been studied. The intercorrelation between the catalytic activity and the method used to obtain ferrites has been shown: the products formation rates are higher in the samples obtained by a ceramic technology, while the sol-gel method makes it possible to obtain ferrites with a greater hydrogen selectivity, which is accounted for by their nanocrystalline state and porous structure. It is shown that the specific catalytic activity of the catalysts, which are prepared by the same method and are of approximately the same chemical composition, is constant. It is shown that a nonisovalent replacement of gadolinium by strontium causes symmetry lowering in the perovskite structure and the appearance of a heterovalent state of iron atoms, which affects ferrite catalytic activity.

DOI: 10.1134/S1995078017020112

INTRODUCTION

In the sphere of oil conversion there is stable growth in interest in alternative technologies that can be used for the preparation of a synthesis gas, because it plays a key role both in the production of motor fuels and in other chemicotechnological processes.

Three methods for oxidative conversion of methane into synthesis gas are used now [1]:

1. Steam reforming of methane (SRM):

$$CH_4 + H_2O \leftrightarrow CO + 3H_2;\ \Delta H^\circ_{298} = +206\ \text{kJ/mol}. \quad (1)$$

2. Partial oxidation of methane (POM):

$$CH_4 + 1/2O_2 \leftrightarrow CO + 2H_2;$$
$$\Delta H^\circ_{298} = -35.6\ \text{kJ/mol}. \quad (2)$$

3. Dry (carbon dioxide) reforming of methane:

$$CH_4 + CO_2 \leftrightarrow 2CO + 2H_2;$$
$$\Delta H^\circ_{298} = -247\ \text{kJ/mol}. \quad (3)$$

To obtain it, the steam reforming of methane is used in industry. However, this method possesses a number of disadvantages, the most substantial of which are the high economic expenditures of its implementation, as a result of which the cost of the synthesis gas obtained by this technology amounts to about two-thirds of the cost of the final products (methanol or dimethyl ether) [1–3].

The DRM process possesses a great potential economic benefit and ecological superiority (utilization of greenhouse gases—methane and carbon dioxide) when compared to SRM and POM. This process makes it possible to obtain synthesis gas with a lower ratio of H_2/CO in an interval of 2 : 1 to 1 : 1. Just such a low ratio of H_2/CO is required for many technologies (the production of hydrocarbons according to the Fisher–Tropsh method; hydroformylation; and the production of methanol, formaldehyde, dimethyl ether, and many other organic compounds). Any improvement in the process to be used to obtain synthesis gas is a topical problem. Special attention is paid to the search for selective stable catalysts, which can operate almost without deactivation due to coke formation [2–5].

The deposited catalysts containing metals of a subgroup Pt or Co, Ni, Fe are efficient, but their main disadvantage is associated both with the high cost of the samples and susceptibility to poisoning.

In these latter years, much attention is paid to complex oxides with a layered perovskite-type structure which possesses a combined oxygen–ion and electron conductance; therefore, due to their high activity and stability they find application as catalysts for high-

temperature processes. For example, when $Ce_{1-x}Ni_xO_y$ ($x = 0.05–0.6$) were used as the catalysts of partial oxidation of methane [6] in a region of 973–1173 K, the hydrogen selectivity reached 80% at the ratio $H_2/CO = 2$. By studying the catalytic activity of $LaCo_{0.8}Cu_{0.2}O_3$ and $LaCoO_3$ [7] in this process, it was shown that on copper-substituted perovskites the conversions of methane possessed higher values. The introduction of copper also suppressed carbon deposition on the catalyst. The authors of [8] found high catalytic activity and stability of lanthanum nickelates, $LaNiO_3$, in the processes of oxidation of methane by a mixture of $CO_2–O_2$. In DRM the samples of $BaZr_{1-x}Me_xO_3$ (Me = Ru, Rh, Pt) have shown high stability and minimal carbonization, while the rhodium-containing oxide possessed the highest catalytic activity [9]. By studying perovskite-type oxides with a composition of $La_{1-x}Sr_xFeO_3$ ($x = 0$, 0.3, 0.5, 0.9) [10] in the process of DRM for all the samples, the ratio $H_2 : CO$ approximately amounted to 2 : 1, while a partial replacement of La by Sr/Ca in the samples of $La_{0.9}M_{0.1}Ni_{0.5}Fe_{0.5}O_3$ resulted in an increase in the conversions of methane and carbon dioxide [11]. It was also found that the introduction of Fe into the structure of a complex oxide leads to an increase in the resistance against carbonization [11].

This work was aimed at studying the possibility of using perovskite-type ferrites, gadolinium and strontium, as catalysts for DRM $A_{n+1}Fe_nO_{3n+1}$, A = Gd, Sr ($n = 1, 2, ..., \infty$) as well as studying the effect of the method of their production and composition on their catalytic activity.

EXPERIMENTAL

As the catalysts of DRM, perovskite-type ferrites were studied: a complex oxide $GdFeO_3$ with the structure of perovskite and perovskite-type layered oxides $GdSrFeO_4$ and $Gd_2SrFe_2O_7$ synthesized according to the ceramic and sol-gel technologies whose methods are described in [12–14].

The results of the synthesis were controlled by the X-ray diffraction (XRD). XRD was performed on a Thermo ARL X'TRA and Rigaku MiniFlex II diffractometers using CuK_α radiation. The PDF2 database was used to identify the results.

The presence and character of thermal effects arising by heating the samples were studied by the method of synchronous thermal analysis using a Netzsch STA449 F1 Jupiter device conjugated with a Netzsch QMS 403 quadrupol mass spectrometer with Aeolos for analyzing the evolved gases. The measurements were carried out in a temperature range of 298–1273 K with a rate of heating of 10 K/min.

Three independent methods were used to determine the size of the particles:

1. X-ray diffraction of crystals, which makes it possible to estimate the size of the coherent scattering region according to the Scherrer formula.

2. Scanning electron microscopy (a Zeiss EVO®40 electron microscope with an accelerating voltage of 10 kV and resolution of 3 nm, which works in the mode of low vacuum and does not need sputtering for nonconducting samples, and a Carl Zeiss Supra 40VP electron microscope with a voltage of 20 kV and resolution of 1.3 nm).

3. Photon correlation spectroscopy (a Malvern Zetasizer Nano analyzer with a helium–neon laser of 4 mW power and a wavelength of 633 nm). The size distributions of particles were obtained from the analysis of the correlation functions using the Multiple Narrow Modes algorithm of the analyzer software.

The surface properties of the samples were measured via the low–temperature adsorption of nitrogen at $T = 77$ K on a Nova 4200E instrument (Quantachrome). The obtained adsorption–desorption isotherms were used to study the specific surfaces of the samples via BET method and the sizes of pores.

The states of iron atoms in all the samples were studied by Mössbauer spectroscopy. The spectra were recorded at room temperature on a spectrometer Wissel (^{57}Co in the rhodium matrix with an activity of 10 mKu); the isomer shifts were calculated with respect to α-Fe. In order to estimate the fraction of iron atoms in different states, the intensity of the signals was determined to an accuracy of the coefficient of resonance absorption.

The catalytic activity of the samples was determined by delivering the gaseous mixture at a ratio of the components of $CO_2 : CH_4 = 1 : 1$. The studies were carried out in a flow catalytic device at the atmospheric pressure and volume rates of 0.5–1.0 L/h in a temperature interval of 773–1223 K. The catalysts with a mass of about 100 mg were placed into a quartz reactor with a diameter of 1 cm. An analysis of the products was carried out by the chromatographic method on the Crystal 2000M device (column with a Porapak Q; detectors of thermal conductivity and flame–ionization). The values of the conversions and rates of methane and carbon dioxide expenditures and the rates at which the products of reactions were formed (the specific catalytic activity (SPA)) at each preset temperature were measured after achieving a stationary state, which was manifested by the constancy of the chromatographic peak areas and were calculated per unit mass of the catalyst.

The numbers of mols of reagents and products in the analyzed dose were determined with the use of regression equations of the type

$$n_i = k_i S_i, \quad (4)$$

where n_i is the number of moles of the ith substance in the analyzed dose; S_i is the area of the ith peak, mV min; and k_i is the coefficient of linear regression for the ist substance, mol min/mV.

The rates of exposure of reagents (ω_i, mol/(h m^2)) and the formation of the products (w_i, mol/(h m^2)) were calculated by formulas (2) and (3), respectively:

$$\omega_i = \frac{(n_i^0 - n_i)w}{VmS_{sp}}, \quad (5)$$

$$w_i = \frac{n_i w}{VmS_{sp}}, \quad (6)$$

where n_i is the amount of the ith product in a gaseous phase, mol; n_0 is the initial amount of the ith product in the reaction mixture mol; w is the volume rate of the reaction mixture, L/h; V is the volume of the chromatograph loop, 0.153×10^{-3} L; m is the catalyst mass, g; and S_{sp} is the spesific surface area of the catalyst, m^2/g.

The conversions (α_i) CH_4 and CO_2 were calculated by the formula

$$\alpha_i = \frac{(n_i^0 - n_i)}{n_i^0} \times 100\%, \quad (7)$$

where n_i is the amount of CH_4 or CO_2 in a gaseous phase, mol; n_i^0 is the initial amount of the ith product in the reaction mixture, mol.

The error in the determination of each component did not exceed 5 rel % and was composed of the error of temperature determination and the error in the measurement of the reaction mixture delivery rate.

The hydrogen selectivity S was calculated as the ratio of the produced hydrogen amount to the general amount of reacted methane

$$S_{H_2} = \frac{n(H_2)_{form}}{2n(CH_4)_{react}} \times 100\%. \quad (8)$$

The carbon monoxide selectivity S was calculated as the ratio of the formed CO amount to the general amount of reacted methane and CO_2:

$$S_{CO} = \frac{n(CO)_{form}}{n(CH_4)_{react} + n(CO_2)_{react}} \times 100\%. \quad (9)$$

The catalytic activity of the oxides $GdFeO_3$, $GdSrFeO_4$, and $Gd_2SrFe_2O_7$ synthesized by two methods was studied in comparison with the activity of Fe_2O_3 and $SrFeO_{3-x}$.

RESULTS AND DISCUSSION

The perovskite-type layered oxides $GdSrFeO_4$ and $Gd_2SrFe_2O_7$ belong to the Raddlesden–Popper phases $A_{n+1}Fe_nO_{3n+1}$, n = 1, 2 [15]. These layered structures are built according to a block principle from interpenetrating fragments of the perovskite structure ABO_3 (P) and the structure of rock salt AO (RS) with a succession of alternation of the layers ...(P)(RS)(P)(RS)... and ...(P)(P)(RS)(P)(P)(RS). Finally, at $n = \infty$, the structure of perovskite takes place—oxide $GdFeO_3$ (Fig. 1).

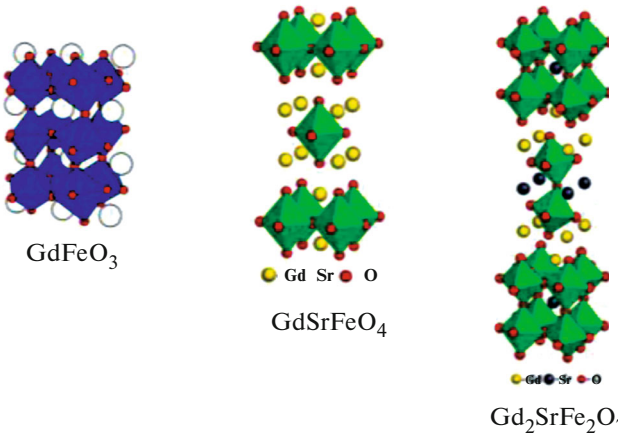

Fig. 1. (Color online) Structures of distorted perovskite ferrite $GdFeO_3$ and layered oxides $GdSrFeO_4$ and $Gd_2SrFe_2O_7$ (cations Fe^{3+} are in an octahedral ambience of oxygen atoms).

Using the method of X-ray diffraction, it was found that all the samples synthesized both by a high-temperature solid-phase synthesis and by sol-gel method are single-phase (Fig. 2). The determination of the coherent scattering region (CSR) has shown that the crystallites of the samples obtained by sol-gel technology are of about 50 nm. The results of scanning electron microscopy indicate that the sol-gel technology makes it possible to reduce the sizes of particles of the ferrites $GdFeO_3$, $GdSrFeO_4$, and $Gd_2SrFe_2O_7$ from 10 μm, which were obtained by the ceramic technology, to 200 nm (Fig. 3). The particles that were obtained are anisotropic, the length of crystals amounts to 100–200 nm, and the diameter is on the order of 50 nm (Fig. 3). The photon correlation spectroscopy registers the average size of the particles on the order of 200–250 nm, which is close to the particle length. The scanning electron microscopy reveals a different morphology of the particles obtained by different methods: the particles obtained by sol-gel technology possess a more regular shape and approximately the same size and are porous agglomerates.

Table 1 presents the average particle values, the specific surface area, and the characteristics of porosity for all the samples that were studied. In general, it is shown that the samples synthesized by the ceramic technology are in a submicrocrystalline state, while those obtained by sol-gel method are in nanocrystalline state. A study using the Mössbauer spectroscopy

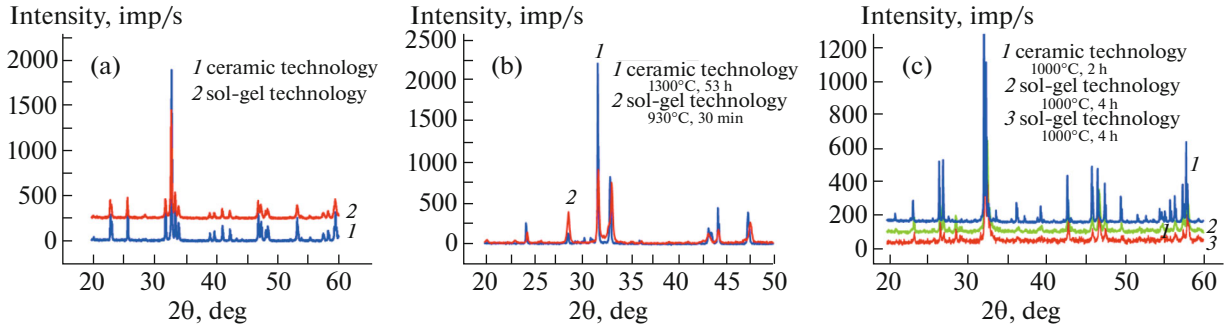

Fig. 2. (Color online) Diffractograms of complex ferrites: (a) $GdFeO_3$ ((*1*) ceramic technology; (*2*) sol-gel technology; no. maps PDF2 01-072-9906), (b) $GdSrFeO_4$ ((*1*) ceramic technology, 1300°C, 53 h; (*2*) sol-gel technology, 930°C, 30 min; no. maps PDF2 00-025-0903 ($NdSrFeO_4$)), (c) $Gd_2SrFe_2O_7$ ((*1*) ceramic technology 1400°C, 78 h; (*2*) sol-gel technology, 1000°C, 4 h; (*3*) sol-gel technology, 1000°C, 2 h; no. maps PDF2 01-089-1088).

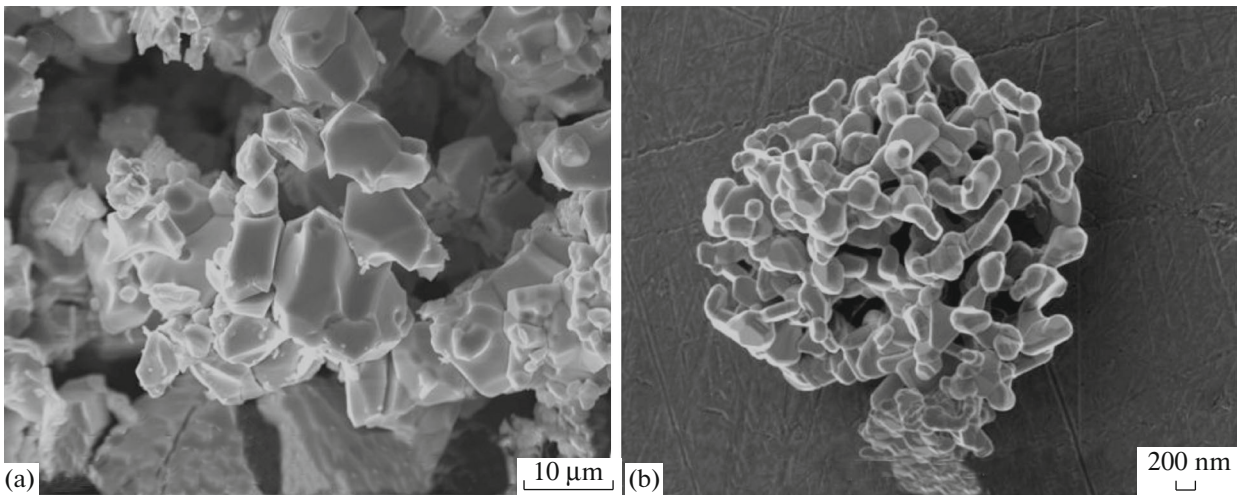

Fig. 3. Microphotography of complex layered oxide $Gd_2SrFe_2O_7$ obtained (a) by ceramic technology and (b) by sol-gel technology.

of complex ferrites obtained by sol-gel technology made it possible to reveal in $GdFeO_3$ samples iron atoms in the state Fe^{+3}, in two fields of different symmetry, and in complex oxides $GdSrFeO_4$ and $Gd_2SrFe_2O_7$ a coexistence of two forms of iron: Fe^{+3} and Fe^{+4}. A study of the compounds obtained by the ceramic technology has shown the presence of a heterovalent state of iron atoms only for the $SrFeO_{3-x}$ sample, in contrast to $GdFeO_3$ and $Gd_2SrFe_2O_7$, in which iron atoms are in a single state: Fe^{+3}. The Mössbauer spectra were partially described in [13, 16], while the parameters of their components are presented in Table 1.

Thermal analysis has shown that all the catalysts are thermally stable in the temperature interval in which the catalytic properties were studied.

The results of studying the catalytic activity in the DRM reaction (Fig. 4, Table 2) have shown that, when a complex oxide $GdFeO_3$ was used, which was obtained by the ceramic technology, the consumption rate of the reactants (CH_4 and CO_2) and the formation rate of hydrogen and carbon monoxide achieved higher values compared to those for a ferrite synthesized by the sol-gel method, as well as compared to Fe_2O_3 oxide. At $T = 1223$ K, $W(H_2)$ for $GdFeO_{3(s\text{-}g)}$ and $GdFeO_{3(cer)}$ were equal to 0.018 and 0.066 mol/(h m^2), respectively; W (CO) for $GdFeO_{3(s\text{-}g)}$ and $GdFeO_{3(cer)}$ – 0.03 and 0.18 mol/(h m^2). At the same time, for methane and carbon dioxide conversion, an opposite trend was observed: $\alpha(CH_4)$ and $\alpha(CO_2)$ in the presence of $GdFeO_{3(s\text{-}g)}$ catalyst at 1223 K achieved 51 and 71%, respectively, (Fig. 4) and exceeded by several times the values obtained on a ceramic sample.

It should be noted that, in the process of reaction, the catalyst Fe_2O_3 deactivated due to its surface carbonization.

The replacement of gadolinium by strontium (transition from $GdFeO_3$ to $SrFeO_{3-x}$) resulted in a reduc-

Table 1. Values of the specific surface area, size, and volume of pores and parameters of the Mössbauer spectra of complex oxides $GdFeO_3$, $SrFeO_{3-x}$, $GdSrFeO_4$, and $Gd_2SrFe_2O_7$

Sample	D_{ap}, μm	S_{sp}, m^2/g	V, cm^3/g	$\bar{r}_{por}$, nm	Fe^{n+}	δ, mm/s	χ, %
$GdFeO_{3\ (s\text{-}g)}$	0.05	7.5	0.004	3.0	Fe^{+3}	0.12	6
					Fe^{+3}	0.36	94
$GdSrFeO_{4\ (s\text{-}g)}$		4.8	0.001	2.0	Fe^{+4}	0.09	17
	0.1				Fe^{+3}	0.27	33
					Fe^{+3}	0.17	30
					Fe^{+3}	0.37	20
$Gd_2SrFe_2O_{7\ (s\text{-}g)}$	0.2	4.4	0.001	2.2	Fe^{+4}	0.07	13
					Fe^{+3}	0.36	87
$SrFeO_{3-x\ (cer)}$		0.4	–	–	Fe^{+4}	–0.24	27
					Fe^{+3}	0.29	55
	≈10				Fe^{+3}	0.49	18
$GdFeO_{3\ (cer)}$		0.7	–	–	Fe^{+3}	0.36	100
$Gd_2SrFe_2O_{7\ (cer)}$		0.2	–	–	Fe^{+3}	0.34	100

Denotations: D_{ap} average size of the particles, μm; S_{sp} specific surface area of the samples, m^2/g; V volume of the pores, cm^3/g; $\bar{r}_{por}$ average size of the pores, nm; δ chemical shift, mm/s; and χ content of iron ions Fe^{n+}, %.

Table 2. Conversions and consumption rates of methane and carbon dioxide, H_2 and CO products formation rates and hydrogen and carbon monoxide selectivity at $T = 1223$ K for the gadolinium and strontium ferrites under study

Number of perovskite layers	Sample	$T = 1223$ K								
		α (CH_4), %	α (CO_2), %	w (CH_4), mol/(h m^2)	w (CO_2), mol/(h m^2)	w (H_2), mol/(h m^2)	w(CO), mol/(h m^2)	S(H_2), %	S(CO), %	H_2 : CO
–	Fe_2O_3	14	29	0.007	0.014	0.003	0.015	31	52	0.22
$n = \infty$	$GdFeO_{3\ (s\text{-}g)}$	51	71	0.016	0.020	0.018	0.027	57	66	0.68
	$GdFeO_{3\ (cer)}$	26	49	0.086	0.159	0.066	0.186	38	76	0.36
	$SrFeO_{3-x\ (cer)}$	11	29	0.062	0.160	0.035	0.140	28	64	0.25
$n = 2$	$Gd_2SrFe_2O_{7(s\text{-}g)}$	30	49	0.014	0.023	0.007	0.022	33	73	0.29
	$Gd_2SrFe_2O_{7\ (cer)}$	11	20	0.113	0.217	0.035	0.180	16	54	0.20
$n = 1$	$GdSrFeO_{4\ (s\text{-}g)}$	18	34	0.009	0.015	0.006	0.020	31	86	0.27

tion of the catalytic activity of ferrite in DRM reaction. The values of CH_4 and CO_2 conversions and the rates of CH_4 consumption and the H_2 and CO formation in the presence of $SrFeO_{(3-x)\ (cer)}$ appeared to be lower than in the reaction with $GdFeO_{3(cer)}$ catalyst (Table 2).

A complication of the perovskite structure (transition from the perovskite structure to a layered perovskite-type structure) practically did not change the catalytic characteristics. The product formation rates ratio to the specific surface area has shown that the CO activity $GdFeO_{3(s\text{-}g)}$, $Gd_2SrFe_2O_{7(s\text{-}g)}$, and $GdSrFeO_{4(s\text{-}g)}$ were found to be equal to 0.027, 0.020, and 0.022 mol/(h m^2) at 1223 K, respectively. For ceramic samples $GdFeO_{3(cer)}$, $SrFeO_{4(cer)}$, and $Gd_2SrFe_2O_{7(cer)}$ at the same temperature of 1223 K, the CO formation rates were equal to 0.186, 0.140, and 0.180 mol/(h m^2), respectively. Similar trends were observed also for CH_4 and CO_2 (Table 2). This means that the number of the perovskite layers did not affect SPA as concerned methane and carbon oxides, and we can conclude that SPA of the catalysts prepared by the same method and of approximately the same chemical composition is constant.

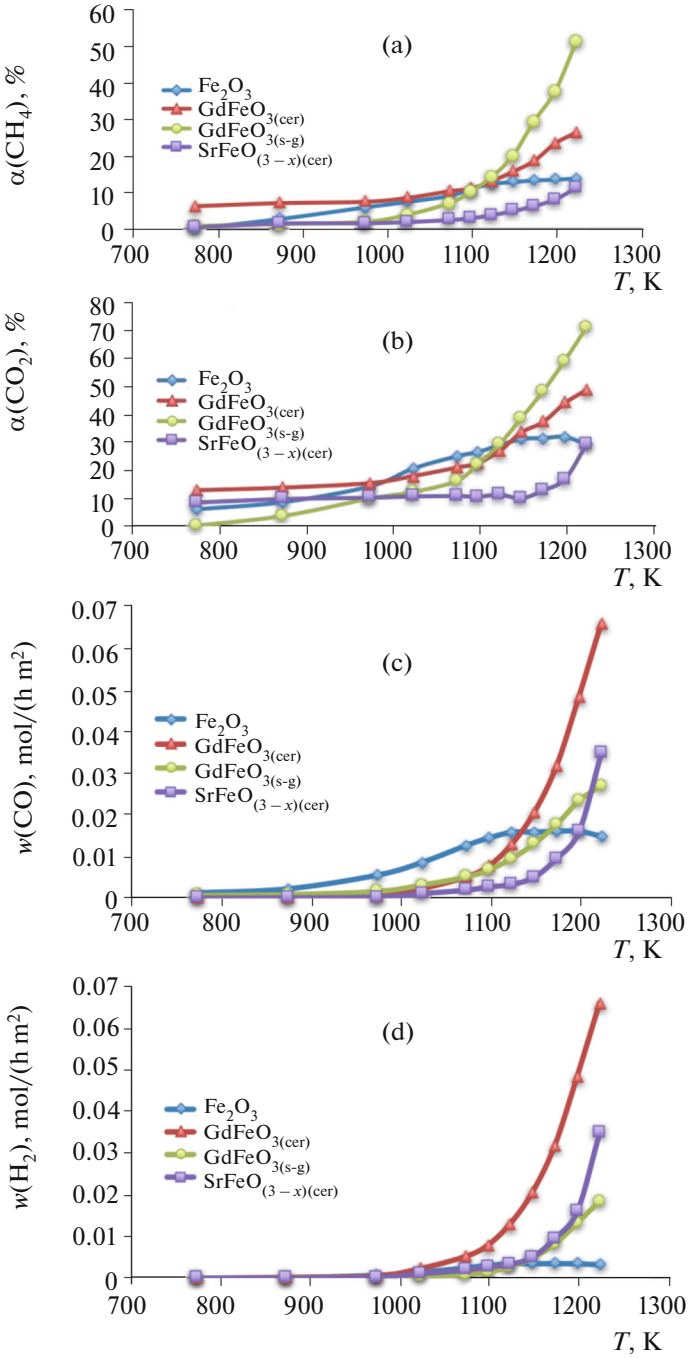

Fig. 4. (Color online) Temperature dependences of methane (a) and carbon dioxide (b) conversions; the formation rate of carbon monoxide (c) and hydrogen (d) at the Fe_2O_3, $GdFeO_{3(cer)}$, $GdFeO_{3(s\text{-}g)}$, and $SrFeO_{(3-x)}$ samples.

A comparative analysis of the catalytic properties of all the samples which we studied has shown that, despite the low rates of product formation in the samples synthesized by the sol-gel method, the reaction selectivity with respect to hydrogen (S_{H_2}) and the ratio $H_2 : CO$ were higher than in the ceramic samples (Table 2). $GdFeO_{3\ (s\text{-}g)}$ showed the highest hydrogen selectivity. A nonisovalent replacement of gadolinium by strontium and an increase of its fraction in complex layered samples $Gd_2SrFe_2O_7$ ($n = 2$) and $GdSrFeO_4$ ($n = 1$) led to a decrease in the reaction selectivity on hydrogen both for sol-gel samples and for ceramic ferrites (Table 2).

Some differences in the catalytic properties of the ferrites synthesized by two different methods can be associated with the peculiarities in the morphology of

Table 3. Experimental energies of activation and preexponential factors for the samples under study

Sample	$E_a(CH_4)$, kJ/mol	$\ln k_0(CH_4)$	$E_a(CO_2)$, kJ/mol	$\ln k_0(CO_2)$	$E_a(CO)$, kJ/mol	$\ln k_0(CO)$	$E_a(H_2)$, kJ/mol	$\ln k_0(H_2)$
$Gd_2SrFe_2O_{7\ (s\text{-}g)}$	93	7.4	123	11.3	145	14.2	230	21.0
$GdFeO_{3\ (s\text{-}g)}$	99	9.1	116	11.6	133	13.9	198	19.3
Fe_2O_3	47	1.4	38	1.3	102	7.3	113	8.1
$GdFeO_{3\ (cer)}$	87	7.5	99	9.7	116	12	156	14.8
$Gd_2SrFe_2O_{7\ (cer)}$	133	10.8	102	13	170	16	204	17.5

the catalyst particles: a submicrocrystalline state of the samples obtained by a ceramic method and nanocrystalline state of the samples synthesized by sol-gel technology. The porous structure of the latter and their large specific surface can promote the chemosorption of reagents, which is manifested in their conversions.

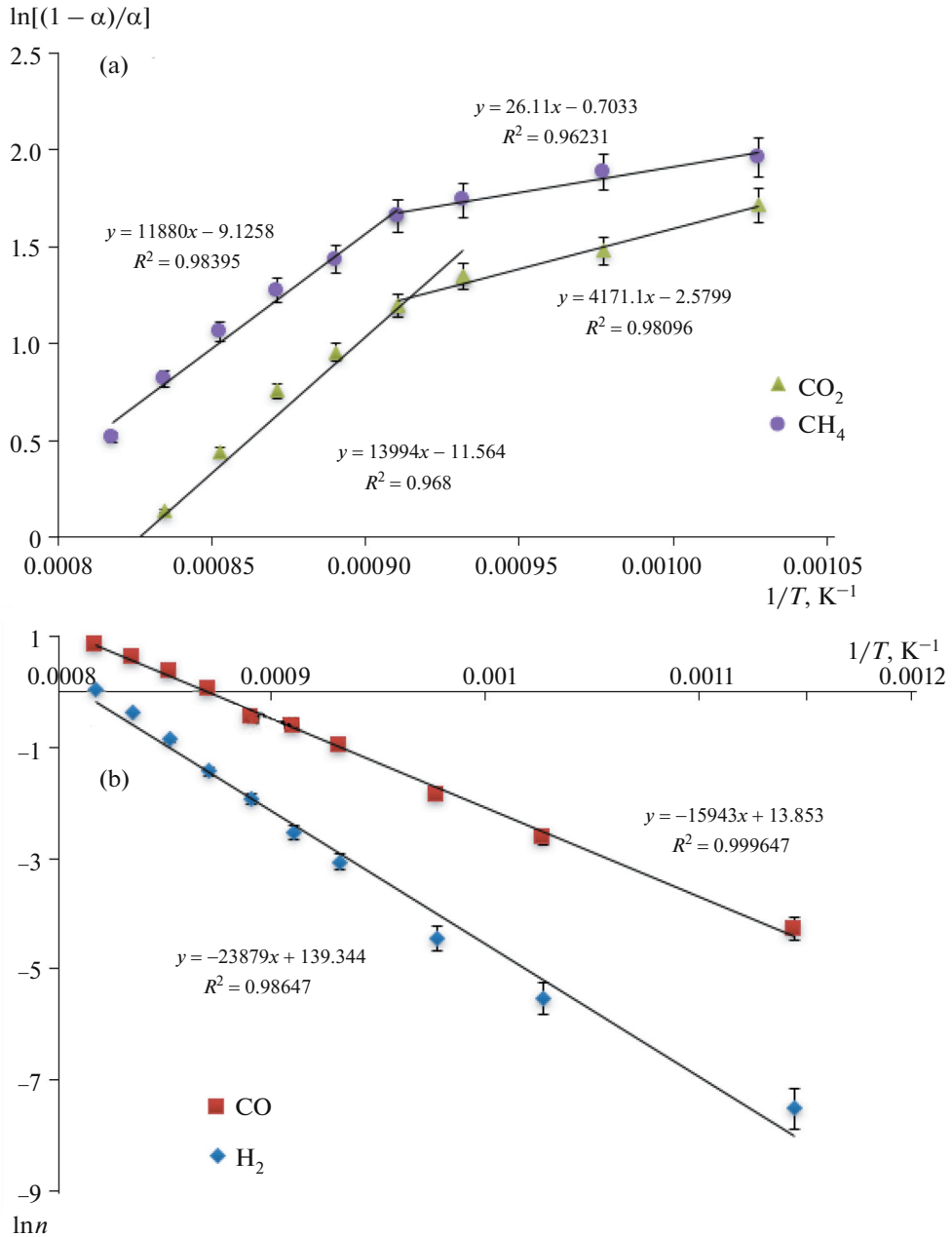

Fig. 5. (Color online) Temperature dependences of the rates of reagent consumption (a) and the formation of the products (b) in linear coordinates of the Arrhenius equation on $GdFeO_3$ sample.

Table 4. Material balance for $GdFeO_{3\,(s\text{-}g)}$ catalyst: amounts of reacted CH_4 and CO_2 and formed CO, H_2, and H_2O in the analyzed dose

Sample	T, K	$n(CH_4)$, μmol	$n(CO_2)$, μmol	$n(CO)$, μmol	$n(H_2)$, μmol	$n(H_2O)$, μmol	Δn_c, μmol
$GdFeO_{3\,(s\text{-}g)}$	973	0.423	0.523	0.071	0.004	0.006	–0.875
	1073	0.512	0.705	0.371	0.047	0.015	–0.846
	1123	0.659	0.953	0.629	0.143	0.038	–0.983
	1173	0.881	1.342	1.404	0.419	0.058	–0.819
	1198	0.801	1.504	1.653	0.508	0.099	–0.652

In order to estimate the values of the efficient activation energies and the number of active surface centers of the ferrites that we studied, the experimental data (the rates of the formation of CO and H_2 and conversion of CH_4 and CO_2) were processed in linear coordinates of the Arrhenius equation [21]. For layered oxides, in contrast to Fe_2O_3, on the Arrhenius dependences for CH_4 and CO_2 (Fig. 5) two regions of linearity were observed with a temperature of transition of $T^* \approx 1000$ K, which is the solution of the system of two linear equations $\ln k = \ln A - \frac{E_a}{R}$ for region 1 ($T < T^*$) and region 2 ($T > T^*$). The presence of two linear regions with different values of the activation energy E_a indicates either a change in the state of the active centers Me^{n+} depending on the temperature or the proceeding of various processes of a complicated reaction in each temperature interval ($T < T^*$, chemosorption of reagents; $T > T^*$, transformation of the chemosorbed complexes into products). Table 3 presents the calculated values of E_a and $\ln k_0$ for the second temperature interval. It can be seen from the table that for the ceramic samples almost all the energies of activation of reagent conversions and the formation of products were lower than the corresponding values obtained for the oxides synthesized by sol-gel method. It is possible to assume that the great SPA of the former is caused by the energy factor. Despite the greatest catalytic activity of the sample $GdFeO_{3(cer)}$, the activation energies of conversions of CH_4 and CO_2 of the formation of H_2 and CO for this ferrite did not possess minimal values at rather large values of the preexponential factor. Furthermore, an increase in the activation energies in other samples was accompanied by a growth of the preexponential factors, which indicates the presence of a certain compensation effect (the Meer–Neidel rule [15, 17]), which is manifested in heterogeneous catalytic reactions. Usually this effect indicates that the reaction under consideration is a multistage one, and, before the establishment of equilibrium in it, a stage of the so-called preequilibrium is achieved, for example, adsorption equilibrium (dissotiative adsorption of methane and the formation of surface carbonate complexes [4]).

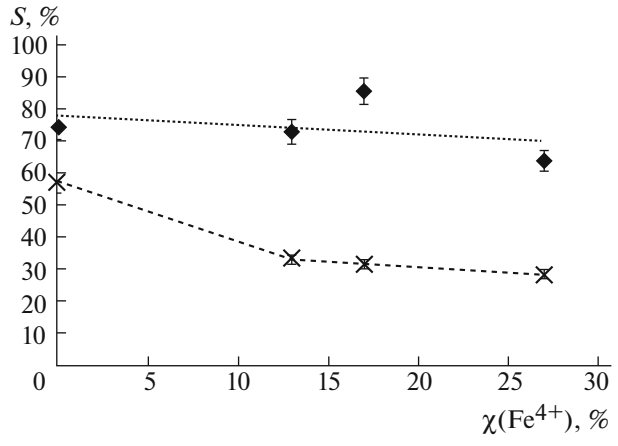

Fig. 6. Dependence of the hydrogen selectivity on the fraction of Fe^{4+} over the $GdFeO_3$, $Gd_2SrFe_2O_7$, $GdSrFeO_4$, and $SrFeO_{3-x}$ samples.

It is shown in [19] that, for heterogeneous-catalytic processes of DRM, $E_a(CO)$ should be larger than $E_a(H_2)$. In our case, an inverse trend is observed: the efficient energies of activation of H_2 formation calculated on the experimental data that we obtained exceed the corresponding values for CO. Water was found among the products of reaction (Table 4) whose amount passed through a maximum by the temperature elevating; the values of H_2/CO are in an interval from 0.2 to 0.7 (Table 2). These facts allow us to assume a parallel (along with DRM) so-called "reverse steam reforming" [19]:

$$CH_4 + CO_2 = 2CO + 2H_2,$$

$$CO_2 + H_2 \leftrightarrow CO + H_2O,$$

$$\overline{CH_4 + CO_2 = 3CO + H_2 + H_2O,}$$

which is suppressed by the temperature elevating. An analysis of the literature data [10, 11, 18–20] has shown that, on the oxide catalysts, the process of DRM proceeds through the formation of intermediate carbonate complexes and their subsequent reduction by C, CH_x-radicals or hydrogen. For all the perovskite catalysts studied by us, $\ln k_0(CO_2) > \ln k_0(CH_4)$, in contrast to iron(III) oxide (Table 3), and since $\ln k_0$ characterizes the amount of the corresponding active centers, it is possible to assume that the process of the

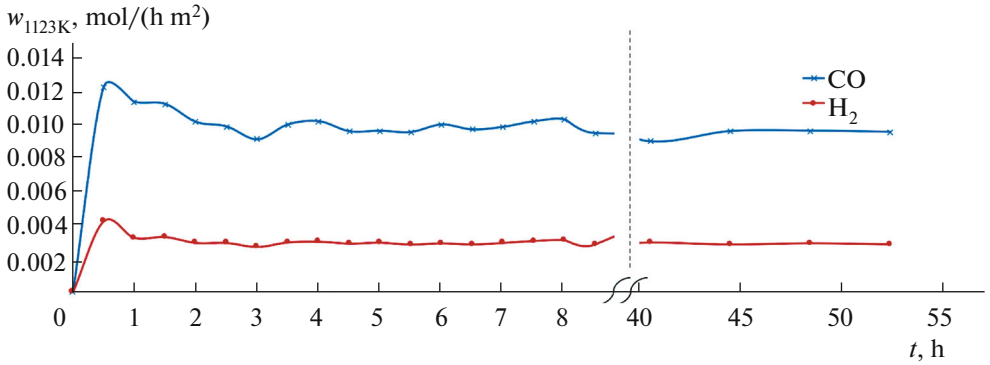

Fig. 7. (Color online) Dependence of the CO and H_2 formation rates on time for $GdFeO_{3\ (s\text{-}g)}$.

(a)

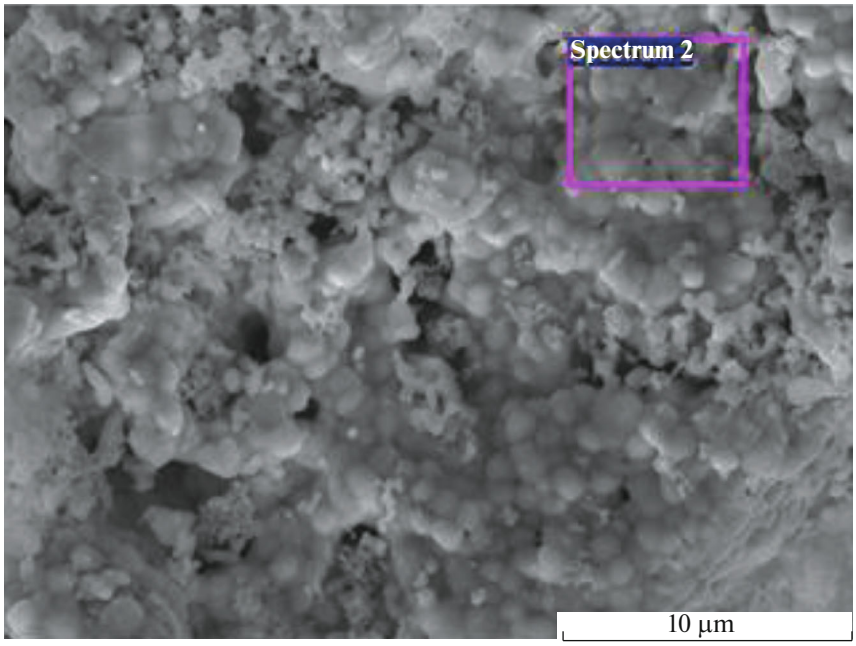

Electron image 1

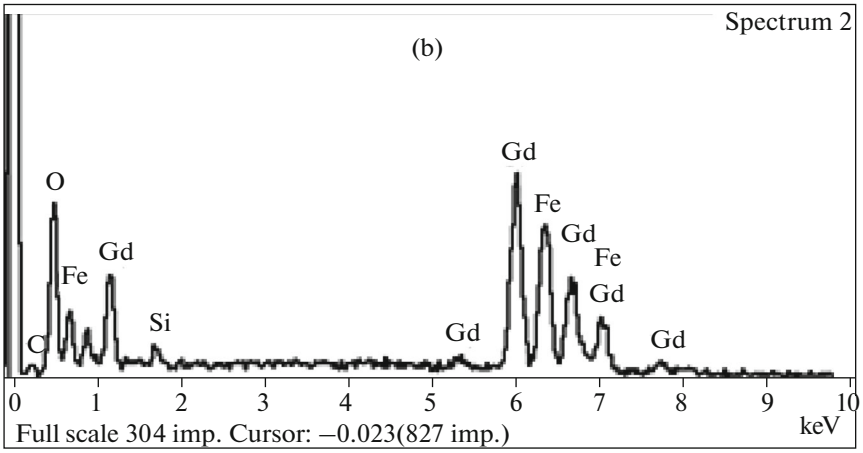

Fig. 8. (Color online) Microphotography (a) and EDX spectra (b) of complex layered oxide $GdFeO_3$ after DRM reaction.

formation of the complexes $M_xO_{y-1}CO_3$ proceeds more intensively than a dissotiative chemosorption of CH_4. This is reflected in the relationship between the reaction products: in all the samples, $w(CO) > w(H_2)$, $S(CO) > S(H_2)$ by inverse ratios of activation energies (Table 3). It is also known that the formation of the atomic hydrogen and CH_x-radicals occurs on iron cations [19, 22, 23]. The described experimental data agree well with the mechanism of the process proposed in [18]:

$$CH_4 + M^1 \rightleftarrows M^1 - CH_4,$$

$$M^1 - CH_4 \rightarrow M^1 - C + 2H_2,$$

$$M^1 - CH_4 \rightarrow M^1 - CH_x + (4 - x)H \rightarrow M^1 - C + 2H_2,$$

$$CO_2 + M_x^2O_y \rightleftarrows M_x^2O_{y-1}CO_3,$$

$$M_x^2O_{y-1}CO_3 + M^1 - C \rightarrow M_x^2O_y + 2CO + M^1.$$

A comparison of the Mössbauer spectroscopy data with the catalytic characteristics of the samples under study proves the assumption of the atomic hydrogen formation on Fe^{+3} centers.

Since the Mössbauer spectra of the oxides synthesized by sol-gel technology revealed the existence of Fe^{+3} in $GdFeO_3$ samples and a coexistence of Fe^{+3} and Fe^{+4} in $GdSrFeO_4$ and $Gd_2SrFe_2O_7$, then a reduction of the hydrogen selectivity and the absence of any influence on the selectivity on CO can be associated with an increase in the fraction of Fe^{+4} from 0 to 27% in the series $GdFeO_3$, $Gd_2SrFe_2O_7$, $GdSrFeO_4$, and $SrFeO_{3-x}$ (Fig. 6). At the same time, in the samples synthesized by a ceramic method, according to the Mössbauer spectroscopy data, iron is only in the state Fe^{+3}; however, the hydrogen selectivity is smaller than for the corresponding samples synthesized by sol-gel technology. This is possibly associated with the different morphology of the catalyst particles, because the porous structure, as was mentioned above, facilitates a dissociative adsorption of CH_4 and spillover of hydrogen from one center to others, despite the smaller fraction of active centers Fe^{+3}.

All the ferrites studied have shown high stability: the catalytic characteristics were kept by carrying out repeated experiments and did not change after 50 h of working (Fig. 7). The data energy dispersive X-ray spectroscopy (EDX) for $GdFeO_3$ sample after the catalytic reaction are shown in Fig. 8 and indicate the presence of carbon on the surface (by estimation data of about 5%). However, all the catalytic characteristics of complex oxides (in contrast to Fe_2O_3) were kept during a long time of working, while Δn_C, characterizing the amount of carbon on the surface, passed through a maximum with the temperature elevating (Table 4). This allows us to assume that the surface carbon is active to a greater degree.

CONCLUSIONS

The catalytic activity of nanostructured perovskite-type ferrites of gadolinium and strontium synthesized by ceramic and sol-gel technologies in the reaction of dry reforming of methane has been studied.

An intercorrelation between the catalytic activity and the method used to obtain ferrites has been shown: the products formation rates are higher for the samples obtained by ceramic technology, while the sol-gel method makes it possible to obtain ferrites with a greater hydrogen selectivity, which is accounted for by their nanocrystalline state and porous structure. It is found that the specific catalytic activity of the catalysts prepared by the same method and of approximately of the same chemical composition is constant. It is shown that an increase in the fraction of Fe^{4+} atoms leads to a decrease in the catalytic activity of a ferrite.

ACKNOWLEDGMENTS

The reported study was partially supported by Russian Foundation for Basic Research (research project nos. 14-03-00940 A and 16-33-00971 mol_a.) and the foundation for facilitating small forms of enterprises in the scientific–technical sphere within the framework of the U.M.N.I.K. competition.

The physicochemical investigations were carried out with the use of equipment of the Thermogravimetric and Calorimetric Methods of Studies and X-ray Diffraction Methods of Studies resource centers, and the Nanotechnologies multidiscipline resource center at St. Petersburg State University.

REFERENCES

1. T. N. Khazova, “Oil and gas chemistry: A strategic kick,” Neftegaz, No. 4, 34–35 (2013).
2. N. Ya. Usachev, V. V. Kharlamov, E. P. Belanova, A. V. Kazakov, T. S. Starostina, and S. A. Kanaev, Pet. Chem. **51**, 96 (2011).
3. K. Liu, C. Song, and V. Subramani, in *Hydrogen and Syngas Production and Purification Technologies* (Wiley-Interscience, New York, 2009).
4. A. Holman, Catal. Today **142**, 2–8 (2009).
5. G. A. Olah, S. Goeppert, and G. K. Prakash, Org. Chem. **74**, 487–498 (2009).
6. W. Shan, M. Fleys, F. Lapicque, D. Swierczynski, A. Kiennemann, Y. Simon, and P.-M. Marquaire, Appl. Catal. A **311**, 24–33 (2006).

7. F. S. Toniolo, R. N. Magalhaes, C. A. Perez, and M. Schmal, Appl. Catal. A **117–118**, 156–166 (2012).
8. A. Garcia, N. Becerra, L. Garcia, I. Ojeda, E. Lopez, and M. R. Goldwasser, Adv. Chem. Eng. Sci. **1**, 169–175 (2011).
9. B. de Caprariis et al., Appl. Catal. A: Gen. **517**, 47–55 (2016).
10. Kun Zhao, Fang He, Zhen Huang, Anqing Zheng, Haibin Li, and Zengli Zhao, Chin. J. Catal. **35**, 1196–1205 (2014).
11. Eun-hyeok Yang, Young-su Noh, S. Ramesh, S. S. Lim, and D. J. Moon, Fuel Process. Technol. **134**, 404–413 (2015).
12. I. A. Zvereva, I. V. Otrepina, V. G. Semenov, E. A. Tugova, V. F. Popova, and V. V. Gusarov, Russ. J. Gen. Chem. **77**, 973 (2007).
13. I. V. Otrepina, V. V. Volodin, I. A. Zvereva, and D. Sh. Liu, Glass Phys. Chem. **35**, 423 (2009).
14. I. V. Chislova, A. A. Matveeva, A. V. Volkova, and I. A. Zvereva, Glass Phys. Chem. **37**, 653 (2011).
15. R. Narayvanan and M. A. El-Sayed, Nano Lett. **4**, 1343 (2004).
16. A. Shilova, I. Chislova, V. Panchuk, V. Semenov, and I. Zvereva, Solid State Phenom. **194**, 116–119 (2013).
17. E. Roduner, *Nanoscopic Materials: Size-Dependent Phenomena* (Inst. Phys. Chem., Univ. Stuttgart, Germany, 2006; Tekhnosfera, Moscow, 2010).
18. Mun-Sing, Ahmad Zuhairi Abdullah, and Subhash Bhatia, ChemCatChem **1**, 192–208 (2009).
19. O. V. Krylov, Zh. Ross. Khim. Obshch. Mendeleeva **44** (1), 19–33 (2000).
20. O. Yamazaki, K. Tomishige, and K. Fujimoto, Appl. Catal. A **136**, 49–56 (1996).
21. S. Z. Roginskii, M. I. Yanovskii, and A. D. Berman, *Fundamentals of the Application of Chromatography in Catalysis* (Nauka, Moscow, 1972) [in Russian].
22. T. F. Sheshko and Yu. M. Serov, Russ. J. Phys. Chem. A **86**, 283 (2012).
23. M. C. J. Bradford and M. A. Vannice, Catal. Rev. **41**, 1–42 (1999).

Translated by R. Litvinov